PERGAMON

International Journal of Heat and Mass Transfer 45 (2002) 2983–2993

International Journal of HEAT and MASS TRANSFER

www.elsevier.com/locate/ijhmt

A fractal permeability model for bi-dispersed porous media

Boming Yu [1], Ping Cheng *

Department of Mechanical Engineering, The Hong Kong University of Science and Technology, Clear Water Bay, Kowloon, Hong Kong

Received 27 October 2000; received in revised form 17 December 2001

Abstract

In this paper a fractal permeability model for bi-dispersed porous media is developed based on the fractal characteristics of pores in the media. The fractal permeability model is found to be a function of the tortuosity fractal dimension, pore area fractal dimension, sizes of particles and clusters, micro-porosity inside clusters, and the effective porosity of a medium. An analytical expression for the pore area fractal dimension is presented by approximating the unit cell by the Sierpinski-type gasket. The pore area fractal dimension and the tortuosity fractal dimension of the porous samples are determined by the box counting method. This fractal model for permeability does not contain any empirical constants. To verify the validity of the model, the predicted permeability data based on the present fractal model are compared with those of measurements. A good agreement between the fractal model prediction of permeability and experimental data is found. This verifies the validity of the present fractal permeability model for bi-dispersed porous media.

Keywords: Fractal; Permeability; Porous media

1. Introduction

In recent years, a great deal of interest has been given in the use of bi-dispersed wick in the evaporators of heat pipes. The bi-dispersed porous structure, as shown in Fig. 1, is composed of clusters (at macro-level), which are agglomerated by small particles (at micro-level). Since the clusters and particles within the clusters are randomly distributed, this leads to macro-pores and micro-pores of various sizes in a bi-dispersed porous medium. Recently, Chen et al. [1] obtained some experimental data on the permeability of bi-dispersed porous media. However, no predictive permeability model is presently available in the literature for bi-dispersed porous media.

The disordered nature of pore structures in bi-dispersed porous media suggests the existence of a fractal structure formed by both the macro-pores between clusters and micro-pores inside clusters. These pores and their distributions are analogous in the microstructures to pores in sandstone [2], to islands or lakes [3] on earth, and to contact spots on engineering surfaces [4–6]. Therefore, it is possible to obtain the permeability of bi-dispersed porous media through a fractal analysis on pore microstructures. Recently, Pitchumani and Ramakrishnan [7,8] presented a fractal geometry model for evaluating permeabilities of porous preforms used in liquid composite molding (LCM). Their fractal model, however, gives some unreasonable results, as pointed out by Yu [9].

In this paper, we focus our attention on the derivation of a fractal model for the permeability of bi-dispersed porous media. In the following, a brief introduction of the fractal theory is first described, and the fractal description of pore structures of a bi-dispersed porous medium is then discussed. A fractal permeability model is derived in terms of the tortuosity fractal dimension, pore area fractal dimension, and porosities of the medium. The determination of the pore area fractal dimension can

* Corresponding author. Tel.: +852-2358-7182; fax: +852-2358-1543.

E-mail addresses: yu3838@public.wh.hb.cn (B. Yu), mepcheng@ust.hk (P. Cheng).

[1] Present address: Department of Physics, Huazhong University of Science and Technology, 1037 Luoyu Rod., Wuhan 430074, China.

0017-9310/02/$ - see front matter
PII: S0017-9310(02)00014-5

Nomenclature

A	area or total area
d_p	diameter of particles
D_e	equivalent diameter of a unit cell
D_f	pore area fractal dimension
D_T	tortuosity fractal dimension
d_0	minimum diameter of a particle
K	total or averaged permeability
L	length scale or length
L_t	capillary length
L_0	representative length
M	area or volume or mass or length of an object
N	number of pores or capillaries
P	pressure
Q	total flow rate
q	flow rate
R	characteristic cluster radius

Subscripts

eff	effective
max	maximum
min	minumum
p	pores
i	micro

Superscript

+	dimensionless

Greek letters

μ	viscosity
ϕ	porosity
λ	hydraulic diameter or pore size

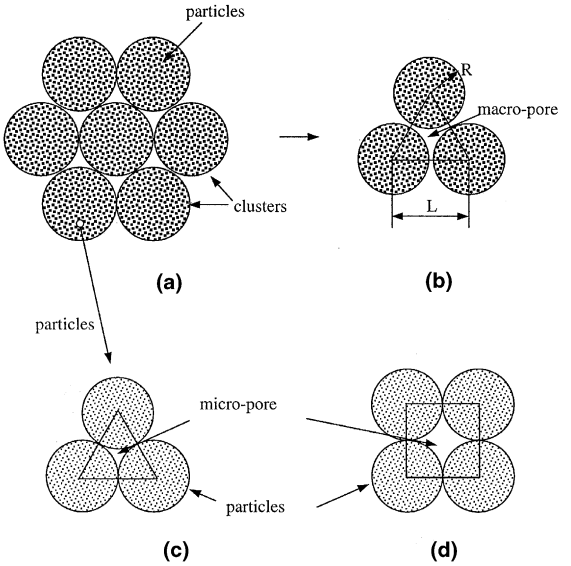

Fig. 1. Schematic of porous media with the bi-dispersed structure: (a) schematic of a bi-dispersed porous medium; (b) an equilateral triangular unit cell; (c) an equilateral triangular unit cell inside clusters; (d) a square unit cell inside clusters.

be obtained based on the two methods: the box-counting method and a theoretical method by approximating the unit cell by the Sierpinski-type gasket [10]. The validity of the proposed fractal permeability model is assessed by a comparison with experimental data.

2. The fractal theory

Euclidean geometry describes ordered objects such as points, curves, surfaces and cubes using integer dimensions 0, 1, 2 and 3, respectively. Associated with each dimension is a measure of the object such as the length of a line, the area of a surface and the volume of a cube. The measures are invariant with respect to the unit of measurement used. However, numerous objects found in nature [3] such as rough surfaces, coastlines, mountains, rivers, lakes and islands, are disordered and irregular, and they do not follow the Euclidean description due to the scale-dependent measures of length, area and volume. These objects are called fractals, and the dimensions of such objects are non-integral and defined as fractal dimensions. The measure of a fractal object, $M(L)$, is related to the length scale, L, through a scaling law in the form of [3]

$$M(L) \sim L^{D_f}, \tag{1}$$

where M can be the length of a line or the area of a surface or the volume of a cube or the mass of an object, and D_f is the fractal dimension of an object. Eq. (1) implies the property of self-similarity, which means that the value of D_f from Eq. (1) is a constant over a range of length scales, L. The geometry structures such as Sierpinski gasket, Sierpinski carpet and Koch curve are the examples of the exact self-similar fractals, which exhibit the self-similarity over an infinite range of length scales [3]. However, exact self-similar fractals in a global sense are rarely found in nature. Many objects found in nature are not exactly self-similar, such as the coastline of an island, they are statistically self-similar. These objects exhibit the self-similarity in some average sense and over a certain local range of length scales, L. The fractal dimension D_f used in this paper is referred to both the statistical and the exact fractals.

3. Fractal characteristics of porous media

A porous medium having various pore sizes can be considered as a bundle of tortuous capillary tubes with variable cross-sectional areas. Let the diameter of a capillary in the medium be λ and its tortuous length along the flow direction be $L_t(\lambda)$. Due to the tortuous nature of the capillary, $L_t(\lambda) \geqslant L_0$, with L_0 being the representative length. For a straight capillary, $L_t(\lambda) = L_0$. Wheatcraft and Tyler [11] developed a fractal scaling/tortuosity relationship for flow through heterogeneous media, and the scaling relationship is given by $L_t(\varepsilon) = \varepsilon^{1-D_T} L_0^{D_T}$, where ε is the length scale of measurement. We argue that the diameter of capillaries are analogous to the length scale ε, which means that the smaller the diameter of a capillary, the longer the capillary. Therefore, the relationship between the diameter and length of capillaries also exhibits the similar fractal scaling law:

$$L_t(\lambda) = \lambda^{1-D_T} L_0^{D_T}, \tag{2}$$

where D_T is the tortuosity fractal dimension, with $1 < D_T < 2$, representing the extent of convolutedness of capillary pathways for fluid flow through a medium. Note that $D_T = 1$ represents a straight capillary path, and a higher value of D_T corresponds to a highly tortuous capillary. The limiting case of $D_T = 2$, corresponds to a highly tortuous line that fills a plane [11]. Eq. (2) diverges as $\lambda \to 0$, which is one of the properties of fractal lines [4]. The tortuosity of a capillary pathway is similar to the triadic Koch teragon [3] which satisfies $L(\varepsilon) = \varepsilon^{1-D}$, where $L(\varepsilon)$ is the length of the triadic Koch teragon whose sides are of length ε. This exact formula is identical with Richardson's empirical law relative to the coast of Britain [3]. Eq. (2) is one of the fractal scaling laws characterizing the fractal properties of pore structures.

Besides the convolutedness of the capillary pathways, the number of capillary pathways with the pore size λ is another important property. The pores in a porous medium are analogous to the islands or lakes on earth. The cumulative size-distribution of islands on the earth's surface follows the power law $N(A > a) \sim a^{-D/2}$ [3], where N is the total number of islands of area (A) greater than a, and D is the fractal dimension of the surface. Majumdar and Bhushan [6] used this power law to describe the contact spots on engineering surfaces, and the power-law relation is

$$N(A \geqslant a) = \left(\frac{a_{max}}{a}\right)^{D_f/2}, \tag{3}$$

where $a_{max} = g\lambda_{max}^2$, $a = g\lambda^2$, with λ being the diameter or pore size and g being a geometry factor. From Eq. (3) the number of islands of area lying between a and $a + da$ is

$$-dN = \frac{D_f}{2} a_{max}^{D_f/2} a^{-(D_f/2+1)}\, da. \tag{4}$$

Since the pores in porous media are analogous to the islands or lakes on earth or spots on engineering surfaces, the cumulative size-distribution of pores or islands should also follow the same fractal scaling law. Thus, Eqs. (3) and (4) can be rewritten as

$$N(L \geqslant \lambda) = \left(\frac{\lambda_{max}}{\lambda}\right)^{D_f} \tag{5}$$

and

$$-dN = D_f \lambda_{max}^{D_f} \lambda^{-(D_f+1)}\, d\lambda, \tag{6}$$

respectively, where D_f, the same fractal dimension [12–14] as in Eq. (1), is the fractal dimension. The negative sign in Eqs. (4) and (6) implies that the island or pore population decreases with the increase of island or pore size, and $-dN > 0$. The number of pores from Eq. (5) becomes infinite as $\lambda \to 0$, which is one of properties of fractal objects [3]. Eq. (5) describes the scaling relationship of the cumulative pore population. Eqs. (1) and (5) hold for both exactly and statistically self-similar fractal geometries. The total number of pores or islands or spots, from the smallest diameter λ_{min} to the largest diameter λ_{max}, can be obtained from Eq. (5) as

$$N_t(L \geqslant \lambda_{min}) = \left(\frac{\lambda_{max}}{\lambda_{min}}\right)^{D_f}. \tag{7}$$

In Eqs. (4)–(6), $1 < D_f < 2$ in the two-dimensional space. Dividing Eq. (6) by Eq. (7) gives

$$-\frac{dN}{N_t} = D_f \lambda_{min}^{D_f} \lambda^{-(D_f+1)}\, d\lambda = f(\lambda)\, d\lambda, \tag{8}$$

where $f(\lambda) = D_f \lambda_{min}^{D_f} \lambda^{-(D_f+1)}$ is the probability density function, which satisfies the following condition

$$f(\lambda) \geqslant 0. \tag{9}$$

As in the probability theory, the probability density function, $f(\lambda)$, should also satisfy the following relationship:

$$\int_{-\infty}^{\infty} f(\lambda)\, d\lambda = \int_{\lambda_{min}}^{\lambda_{max}} f(\lambda)\, d\lambda = 1 - \left(\frac{\lambda_{min}}{\lambda_{max}}\right)^{D_f}. \tag{10a}$$

The above equation becomes

$$\int_{-\infty}^{\infty} f(\lambda)\, d\lambda = \int_{\lambda_{min}}^{\lambda_{max}} f(\lambda)\, d\lambda = 1 \tag{10b}$$

if and only if

$$\left(\frac{\lambda_{min}}{\lambda_{max}}\right)^{D_f} = 0 \tag{11}$$

is satisfied. Eq. (11) implies that $\lambda_{min} \ll \lambda_{max}$ must be satisfied for fractal analysis of a porous medium [15];

otherwise the porous medium is a non-fractal medium. For example, if $\lambda_{\min} = \lambda_{\max}$, both of Eqs. (11) and (10b) do not hold. Therefore, caution must be taken for fractal analysis of porous media, and Eq. (11) can be considered as a criterion whether a porous medium can be characterized by fractal theory and technique [15]. If Eq. (11) does not hold, the porous medium is a non-fractal medium, and the fractal theory and technique are not applicable. In general, $\lambda_{\min}/\lambda_{\max} < 10^{-2}$ in porous media and Eq. (11) holds approximately. Thus, the fractal theory and technique can be used to analyze properties of porous media. Eqs. (1), (2), (5), (6) and (11) form the basis of the present fractal permeability model, which will be derived in the following sections.

4. Fractal permeability for capillary tubes

Consider a unit cell consisting of a bundle of tortuous capillary tubes with variable cross-sectional area. The total volumetric flow rate, Q, through the unit cell is a sum of the flow rates through all the individual capillaries. The flow rate through a single tortuous capillary is given by modifying the well-known Hagen–Poiseulle equation [16] to give

$$q(\lambda) = \frac{\pi}{128}\frac{\Delta P}{L_t(\lambda)}\frac{\lambda^4}{\mu}, \tag{12}$$

where λ is the hydraulic diameter of a single capillary tube, μ is the viscosity of the fluid, ΔP is the pressure gradient, and L_t is the length of the tortuous capillary tube. The total flow rate Q can be obtained by integrating the individual flow rate, $q(\lambda)$, over the entire range of pore sizes from the minimum pore $\lambda_{\min}$ to the maximum pore $\lambda_{\max}$ in a unit cell. According to Eqs. (2), (6) and (12), we have

$$\begin{aligned} Q &= -\int_{\lambda_{\min}}^{\lambda_{\max}} q(\lambda)\,\mathrm{d}N(\lambda) \\ &= \frac{\pi}{128}\frac{\Delta P}{\mu}\frac{A}{L_0}\frac{L_0^{1-D_T}}{A}\frac{D_f}{3+D_T-D_f} \\ &\quad\times \lambda_{\max}^{3+D_T}\left[1-\left(\frac{\lambda_{\min}}{\lambda_{\max}}\right)^{3+D_T-D_f}\right] \\ &= \frac{\pi}{128}\frac{\Delta P}{\mu}\frac{A}{L_0}\frac{L_0^{1-D_T}}{A}\frac{D_f}{3+D_T-D_f} \\ &\quad\times \lambda_{\max}^{3+D_T}\left[1-\left(\frac{\lambda_{\min}}{\lambda_{\max}}\right)^{D_f}\left(\frac{\lambda_{\min}}{\lambda_{\max}}\right)^{3+D_T-2D_f}\right]. \end{aligned} \tag{13}$$

Since $1 < D_T < 2$ and $1 < D_f < 2$, the exponent $3 + D_T - 2D_f > 0$. Also, because $\lambda_{\min}/\lambda_{\max} \sim 10^{-2}$ and $(\lambda_{\min}/\lambda_{\max})^{D_f} \cong 0$, and therefore $0 < (\lambda_{\min}/\lambda_{\max})^{3+D_T-D_f} < 1$. It follows that Eq. (13) can be reduced to

$$\begin{aligned} Q &= -\int_{\lambda_{\min}}^{\lambda_{\max}} q(\lambda)\,\mathrm{d}N(\lambda) \\ &= \frac{\pi}{128}\frac{\Delta P}{\mu}\frac{A}{L_0}\frac{L_0^{1-D_T}}{A}\frac{D_f}{3+D_T-D_f}\lambda_{\max}^{3+D_T}. \end{aligned} \tag{14}$$

The major difference between Eq. (14) and the expression given by Pitchumani and Ramakrishnan [7,8] is that the criterion given by Eq. (11) was not taken into consideration in their model. Furthermore, the results of integrations for the total flow rate and for the permeability in their work [7,8] were found to be in error [9].

Using Darcy's law, we obtain the expression for the permeability of a porous medium as follows:

$$K = \frac{\mu L_0 Q}{\Delta P A} = \frac{\pi}{128}\frac{L_0^{1-D_T}}{A}\frac{D_f}{3+D_T-D_f}\lambda_{\max}^{3+D_T}, \tag{15}$$

which indicates that the permeability is a function of the pore fractal dimension D_f, tortuosity fractal dimension D_T and structural parameters, A, L_0 and $\lambda_{\max}$. If a straight capillary model ($D_T = 1$) is assumed, Eqs. (14) and (15) can be reduced to

$$Q = \frac{\pi}{128}\frac{\Delta P}{\mu}\frac{A}{L_0}\frac{1}{A}\frac{D_f}{4-D_f}\lambda_{\max}^4, \tag{16}$$

$$K = \frac{\pi}{128}\frac{1}{A}\frac{D_f}{4-D_f}\lambda_{\max}^4, \tag{17}$$

respectively. Eqs. (14)–(17) indicate that the flow rate and permeability are very sensitive to the maximum pore size $\lambda_{\max}$. It is also shown that the higher the fractal dimension D_f, the larger the flow rate and the permeability value. From Eqs. (16) and (17), it can be seen that the flow rate and the permeability will reach the possible maximum values as the pore area fractal dimension approaches its possible maximum value of 2. The fractal dimension $D_f = 2$ corresponds to a smooth surface or plane or a compact cluster [3,17–20]. This means that if we consider a smooth surface or a compact cluster or a circle or a square to be the cross-section of a pore, the fractal dimension of the cross-section is 2 and the pore volume fraction of the cross-section is 1. Both the flow rate and the permeability are maximum under such a condition. Thus, for flow through the unit cell with a single capillary tube or pore with $D_f = 2$, we have the maximum flow rate and maximum permeability from Eqs. (16) and (17),

$$Q_{\max} = \frac{\pi}{128}\frac{\Delta P}{L_0\mu}\lambda_{\max}^4 = \frac{D_e^2}{32}\frac{A\Delta P}{L_0\mu}, \tag{18}$$

$$K_{\max} = \frac{\pi}{128}\frac{1}{A}\lambda_{\max}^4 = \frac{D_e^2}{32}. \tag{19}$$

Eq. (18) is exactly the Hagen–Poiseulle equation [16], and the permeability value of $D_e^2/32$ is exactly the expression for flow through a pipe. This indicates that our

model is consistent with the physical situation. Therefore, one can find the flow rate and the permeability for flow through the unit cell with a straight capillary tube either from Eq. (12) by setting $D_T = 1$ (and consequently $L_t = L_0$) or from Eqs. (18) and (19). In comparison, the fractal model presented by Pitchumani and Ramakrishnan [7,8] gives zero total flow rate and zero permeability for $D_f = 2$, which is physically unrealistic.

5. Fractal permeability model for bi-dispersed media

Fig. 1(a) is a schematic of the bi-dispersed porous medium that contains many clusters formed by particle agglomeration. There are two types of pores: macro-pores (on the order of 0.1 cm) between clusters and micro-pores (on the order of 10^{-3} cm) between particles inside each cluster. It is assumed that the size distribution of the macro-pores and the micro-pores is similar, and the tortuosity of flow pathways between clusters and between particles within clusters is also similar. For the present bi-dispersed porous media, we choose an equilateral triangle as a unit cell as shown in Fig. 1(b). Figs. 1(c) and (d) are the schematic of possible micro-configurations of particles, and two configurations (equilateral triangle and square) are assumed. Their micro-porosities are $\phi_i = 1 - \pi/2\sqrt{3} \cong 0.093$ and $\phi_i = 1 - \pi/4 \cong 0.215$, respectively. For the unit cell shown in Fig. 1(b), the effective porosity is given by

$$\phi_{\text{eff}} = \frac{(A - \pi R^2/2) + \phi_i \pi R^2/2}{A}, \tag{20}$$

where A and R are the total area of the unit cell and the average radius of the clusters. Eq. (20) can be solved to give the following expression for the total area of the unit cell:

$$A = \frac{1}{2}\pi R^2 \left[\frac{1-\phi_i}{1-\phi_{\text{eff}}}\right] \tag{21}$$

where the porosity ϕ_{eff} can be measured based on the density method [21] and R can be measured experimentally. Eq. (21) shows that the total area of the unit cell is related to the porosities (ϕ_i and ϕ_{eff}) of the medium and averaged size (R) of the clusters.

The maximum macro-pore area can be calculated from Fig. 1(b) which gives

$$A_{p,\max} = A - \pi R^2/2 = \frac{1}{2}\pi R^2 \left(\frac{1-\phi_i}{1-\phi_{\text{eff}}} - 1\right). \tag{22}$$

The irregular geometry of macro-pore area $A_{p,\max}$ can be approximated as a circle as

$$A_{p,\max} = \pi \lambda_{\max}^2/4. \tag{23}$$

Substituting Eq. (22) into Eq. (23) and solving for $\lambda_{\max}$ give

$$\lambda_{\max} = R\sqrt{2\left(\frac{1-\phi_i}{1-\phi_{\text{eff}}} - 1\right)}, \tag{24}$$

which shows the relation between the macro-pore size in terms of the effective porosity of a medium and the cluster size. Since the flow in the bi-dispersed porous media passes through not only the macro-pores between clusters but also the micro-pores inside clusters, the flow is very complex and may be three-dimensional. When the fluid flows over the clusters, it passes through not only the central-pore but also the narrow gaps (the size is smaller than that of the central-pore) between the adjacent two clusters (see Fig. 2). The unit cell as shown in Fig. 1(b) is correct only for the one-dimensional flow, so is the maximum macro-pore size, $\lambda_{\max}$, given by Eq. (24). Therefore, the gap size between the adjacent two clusters should be taken into account for the macro-pore size. The gap size between the adjacent two clusters can be obtained from the total area of the unit cell as shown in Fig. 1(b), which is given by

$$\Delta L = L - 2R = R\left(\sqrt{\frac{2\pi}{\sqrt{3}}\frac{1-\phi_i}{1-\phi_{\text{eff}}}} - 2\right), \tag{25}$$

where L, the side length of the equilateral triangle unit cell, can be obtained from the relation of $A = \sqrt{3}L^2/4$ where A is also given by Eq. (21). Eq. (25) indicates that the gap size is a function of the porosities ϕ_{eff} and ϕ_i, and the cluster size R. Note that the gap size ΔL given by Eq. (25) is the maximum macro-pore size for the flow around the clusters in a bi-dispersed porous medium, while $\lambda_{\max}$ given by Eq. (24), is the maximum macro-pore size in the direction perpendicular to paper as shown in Fig. 1(b). When the flow through a porous medium, it passes not only through the maximum

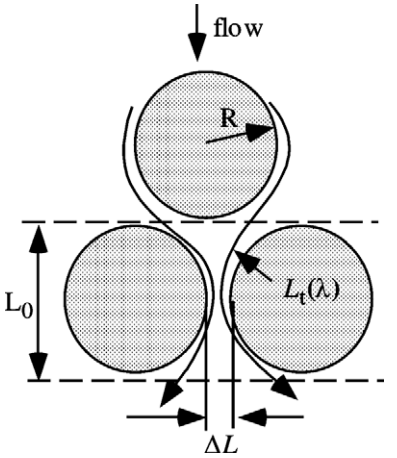

Fig. 2. Schematic of flow through a bi-dispersed medium and its tortuosity.

macro-pores but also through the narrow channels with the width of ΔL. These maximum pores and the narrow channels are in the same direction. Thus, the average maximum macro-pore size of the bi-dispersed porous medium $\bar{\lambda}_{\max}$ is assumed approximately to be

$$\bar{\lambda}_{\max} = (\lambda_{\max} + \Delta L)/2. \tag{26}$$

Finally, we obtain the fractal permeability of a bi-dispersed medium by modifying Eq. (15) as follows:

$$K = \frac{\pi}{128}\frac{L_0^{1-D_T}}{A}\frac{D_f}{3+D_T-D_f}\bar{\lambda}_{\max}^{3+D_T}, \tag{27}$$

where A and $\bar{\lambda}_{\max}$ are determined by Eqs. (21) and (24)–(26), and L_0 is given by

$$L_0 = 2R + \Delta L \tag{28}$$

as is shown in Fig. 2. Note that the fractal permeability given by Eq. (27) does not have any empirical constants. The mono-dispersed porous medium can be considered as a special case of the bi-dispersed porous media by setting $\phi_i = 0$ in the relevant equations. Thus, the permeability of a mono-dispersed medium is also given by Eq. (27) with

$$A = \frac{1}{2}\pi R^2\frac{1}{1-\phi_{\text{eff}}}, \tag{29a}$$

$$\lambda_{\max} = R\sqrt{\frac{2\phi_{\text{eff}}}{1-\phi_{\text{eff}}}}, \tag{29b}$$

$$\Delta L = L - 2R = R\left(\sqrt{\frac{2\pi}{\sqrt{3}}\frac{1}{1-\phi_{\text{eff}}}} - 2\right), \tag{29c}$$

which are obtained from Eqs. (21), (24) and (25) with $\phi_i = 0$. Once the value of the pore area fractal dimension D_f and the tortuosity fractal dimension D_T are found, the permeability of the bi- and mono-dispersed media can be determined. In the next section, we will discuss the determination of the fractal dimensions D_f and D_T.

6. Determination of D_f and D_T

6.1. Evaluation of fractal dimension D_f

We now present two methods for the determination of D_f: one is the box-counting method based on Eq. (5), and the other is the approximation of self-similarity based on the Sierpinski-type gasket model [10].

6.1.1. Box-counting method

The pore area fractal dimension D_f can be determined based on the box-counting method [22]. This method is based on the image analysis of a unit cell or a sufficiently large cross-section of a sample along a plane normal to the flow direction. In this method, the cross-section under consideration is discretized using square boxes of size, λ, then the number, $N(\lambda)$, of boxes required to completely cover the pore areas is counted. The pore area fractal dimension, D_f, can be determined by the value of the slope of a linear fit through data on a logarithmic plot of the cumulative number of pores $N(L \geqslant \lambda)$ versus the pore size λ.

We now apply the box-counting method to determine the pore area fractal dimension D_f of the two bi-dispersed porous samples used by Chen et al. [1]. These bi-dispersed porous samples were made of copper particles with effective porosities of 0.52 and 0.54, respectively. The samples were polished for image analyses under an optical microscope. Fig. 3 shows the image of the bi-dispersed porous sample with the effective porosity of 0.52, where the black and white regions are pores and clusters formed by agglomerated of copper particles, respectively. Since the micro-pores inside clusters are very small and the copper particles are soft, it is difficult to see the micro-pores inside clusters after being polished. The softwares, Photoshop 5.0 and Visual C++5.0, were used to record $N(\lambda) \sim \lambda$ of the macro-pores.

Figs. 4(a) and (b) are the logarithmic plots of the cumulative number of macro-pores versus pore sizes, $N(L \geqslant \lambda) \sim \lambda$, for the two bi-dispersed porous samples with $\phi_{\text{eff}} = 0.52$ and $\phi_{\text{eff}} = 0.54$, respectively. It is seen that the number of cumulative macro-pores decreases as the pore size increases. The data follow a linear relationship on the logarithmic scale, and this confirms the statistical fractal nature of the microstructures of the bi-dispersed porous media. From the slopes of these straight lines we can determine the fractal dimensions

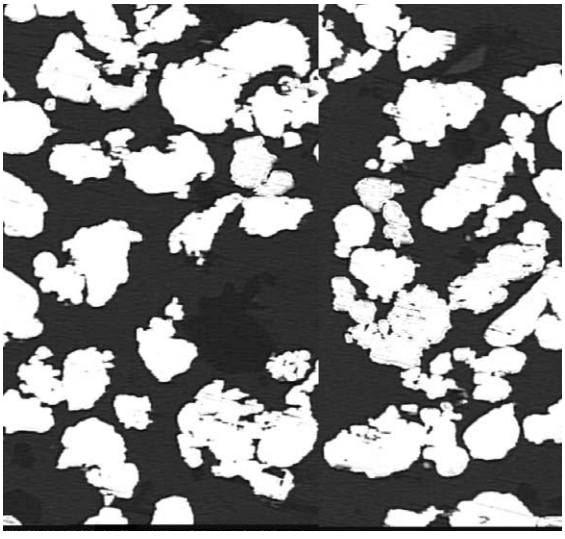

Fig. 3. An image photo of a bi-dispersed sample.

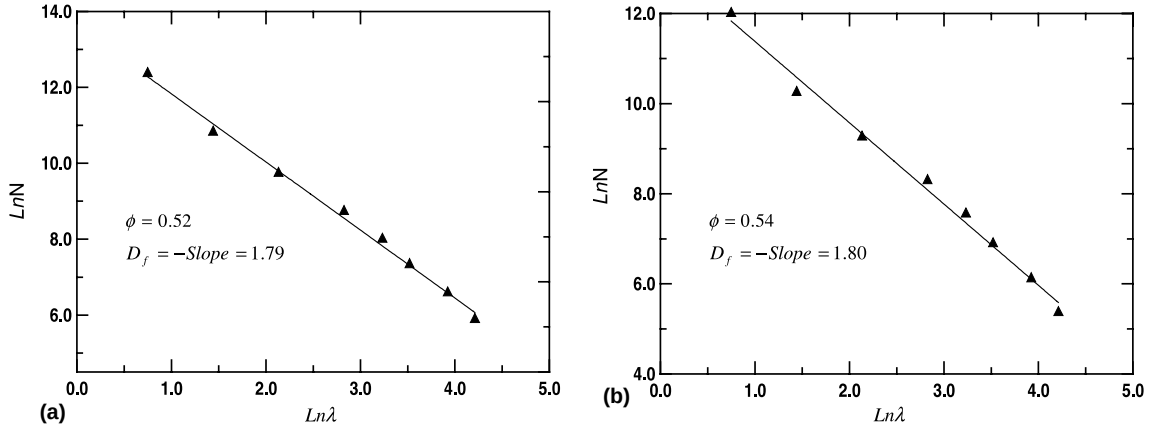

Fig. 4. A logarithmic plot of the cumulative pore number ($N(L \geqslant \lambda)$) versus λ.

$D_f = 1.79$ for the sample with $\phi_{eff} = 0.52$ (Fig. 4(a)) and $D_f = 1.80$ for the sample with $\phi_{eff} = 0.54$ (Fig. 4(b)).

6.1.2. Approximation of the Sierpinski-type gasket

Taking a close look at Figs. 1(a)–(c), we can find the approximate self-similarity existing in the macro-structure between clusters and the micro-structure between particles inside each cluster. This motivates us to use the Sierpinski-type gasket model to simulate the bi-dispersed porous media. The unit cell shown in Figs. 1(b) and (c) can be approximated by the Sierpinski gasket [3] as shown in Fig. 5(a), which is an exact self-similarity fractal geometry. The shaded area fractal dimension is 1.585 ($3 = 2^{D_f}$, $D_f = \ln 3/\ln 2 = 1.585$) [3,10]. However, Fig. 5(a) is only a special case of the Sierpinski-type gaskets with $L = 2$ [10]. Figs. 5(b) and (c) demonstrate the Sierpinski-type gaskets with $L = 3$ and 5, respectively. If the white areas in Figs. 5(b) and (c) are the pores, their respective pore area fractal dimensions are 1.0 ($3 = L^{D_f} = 3^{D_f}$, $D_f = \ln 3/\ln 3 = 1$) and 1.594 ($13 = L^{D_f} = 5^{D_f}$, $D_f = \ln 13/\ln 5 = 1.594$), respectively. Based on the Sierpinski-type gasket structure, the total pore area, including macro-pores and micro-pores for the unit cell as shown in Fig. 1(b), can be approximately calculated by

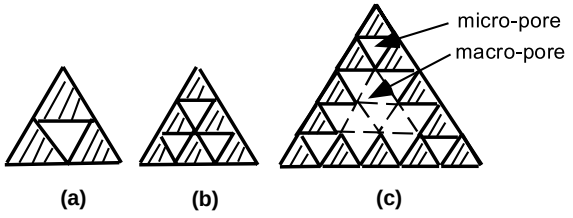

Fig. 5. A Sierpinski-type fractal generator: (a) $L = 2$, (b) $L = 3$, and (c) $L = 5$.

$$A_p = (L^+)^{D_f}, \tag{30}$$

where A_p is the dimensionless total pore area and $L^+ = L/d_0$ with d_0 being the minimum particle diameter within a cluster. It follows from the above equation that

$$D_f = \ln A_p/\ln L^+. \tag{31}$$

To obtain the expression for L^+, we note that the effective porosity of the unit cell can be expressed as

$$\phi_{eff} = A_p/A^+, \tag{32}$$

where the dimensionless total area of the unit cell A^+ can be written as

$$A^+ = (L^+)^2 \tag{33}$$

or

$$L^+ = \sqrt{A^+} = d^+\sqrt{\frac{1-\phi_i}{2(1-\phi_{eff})}} \tag{34}$$

with $d^+ = 2R/d_0$, $A^+ = A/(\pi d_0^2/4)$, where A is given by Eq. (21). Combining Eqs. (31)–(34) yields

$$D_f = 2 + \frac{\ln \phi_{eff}}{\ln\left(d^+\sqrt{(1-\phi_i)/(2(1-\phi_{eff}))}\right)}. \tag{35a}$$

Setting $\phi_i = 0$ in Eq. (35a) gives

$$D_f = 2 + \frac{\ln \phi_{eff}}{\ln\left(d^+\sqrt{(1/2(1-\phi_{eff}))}\right)}, \tag{35b}$$

which is the fractal dimension for mono-dispersed porous media. Eqs. (35a) and (35b), with no other empirical constant, reveals that the pore area fractal dimension is a function of porosities (ϕ_{eff}, ϕ_i), the average cluster size R, and the minimum particle diameter d_0. Although the values of ϕ_{eff} and R can easily be measured, the values of d_0 and ϕ_i are difficult to

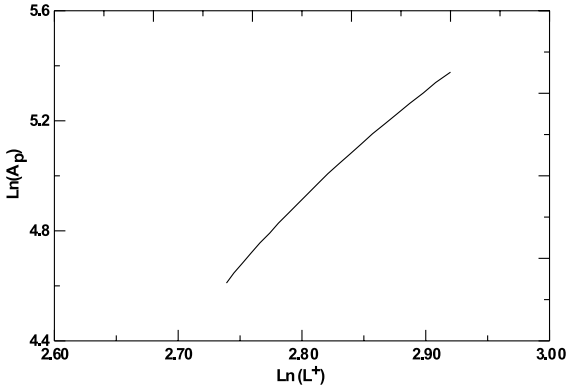

Fig. 6. A logarithmic plot of the total pore area versus L^+.

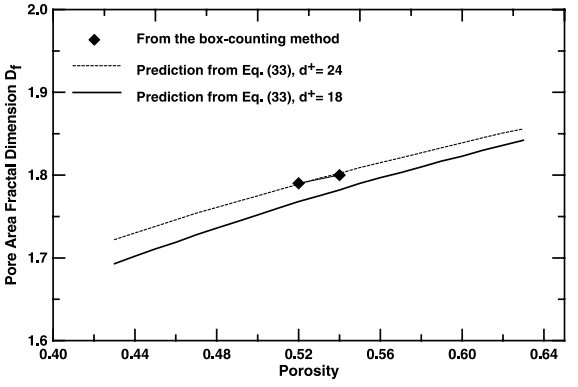

Fig. 7. A comparison of the different methods for the fractal pore area dimension D_f versus porosity and relative cluster size d^+.

measured in practice. Eqs. (35a) and (35b) shows that $D_f = 2$ for $\phi_{eff} = 1$, and vice versa. This is as expected and is consistent with the physical situation. Eqs. (35a) and (35b) also shows that the smaller the cluster the lower the fractal dimension because $\phi_{eff} < 1$ and $\ln \phi_{eff}$ is a negative value. It should be noted that although the Sierpinski-type gasket model is applied to obtain the fractal dimension and porosities of the bi-dispersed porous medium in this paper, it cannot be applied to obtain the permeability of a bi-dispersed porous medium since the flow pathways in bi-dispersed media are not straight.

Fig. 6 is a logarithmic plot of the total pore area A_p given by Eq. (32) versus the length scale L^+ given by Eq. (34). Note that both of these quantities are a function of the effective porosity ϕ_{eff}. Since the values of d_0 and ϕ_i are difficult to measure exactly, we use $d^+ = 24$ and ϕ_i is computed according to $\phi_i = 0.342\phi_{eff}$ [23]. The value of ϕ_i thus computed falls in the range of $0.093 < \phi_i < 0.215$, i.e., the micro-porosities shown in Figs. 1(c) and (d). According to Eq. (30), the local slope of $\ln(A_p)$ versus $\ln(L^+)$ gives the value of D_f at a specific value of L^+. It is shown that the slope of the curve in Fig. 6 is decreasing as the value of L^+ is increased, i.e., as the effective porosity decreases according to Eq. (34). It is found that the average slope in the range of $0.43 < \phi_{eff} < 0.63$ is $D_f = 1.76 \pm 0.08$, which is the average fraction dimension in this range of the effective porosity. This value compares favorably with the values of $D_f = 1.79$ at $\phi_{eff} = 0.52$ and $D_f = 1.80$ at $\phi_{eff} = 0.54$ from the box-counting method.

In Fig. 7, we plot the values of D_f versus the effective porosity. The data points are the values determined by the box-counting method and the lines are the results computed from Eq. (35a). As shown in Fig. 7, if $d^+ = 24$ was used for computation, the value of D_f matches with the values obtained from the box-counting method. To see the effect of d^+ on D_f, computations were also carried for $d^+ = 18$ and the results are also presented in Fig. 7. It is shown that the smaller the relative cluster size, d^+, the lower the fractal dimension. The reason is that the smaller the cluster, the smaller the total area at fixed ϕ_{eff}, which results in the decrease of the total pore area and consequently, the decrease of the fractal dimension. From Fig. 7 it can also be seen that the pore area fractal dimension will approach its possible maximum value of 2 as the porosity reaches the value of 1. This is as expected and is consistent with the actual physical situation, which verifies the present fractal dimension model.

6.2. Evaluation of tortuosity fractal dimension D_T

Since we have assumed that there is a similarity of tortuosity of flow pathways between clusters and between particles within clusters, thus, we need to determine only the tortuosity of pathways between clusters. Because the tortuosity of flow paths between clusters is very similar to the streamtubes [11] in heterogeneous media or coastlines and is described by Eq. (2), therefore, the tortuosity dimension D_T can also be determined by the box-counting method.

Fig. 8 presents five random flow pathways between clusters in the porous sample shown in Fig. 3, where the flow is assumed under a pressure gradient from left to right. The same software that was used for finding D_f based on the box-counting method is now applied to find the tortuosity fractal dimension D_T for these five flow pathways. Fig. 9 shows a plot of $\ln L_t(\lambda)$ versus $\ln \lambda$ for the pathway shown in Fig. 8(e), in which the fractal dimension can be determined from the slope of the straightline that gives $D_T = 1.12$. Similarly, the values of D_T from the other four pathways are found to be 1.07, 1.08, 1.09 and 1.13, respectively. Thus, the averaged values of the tortuosity fractal dimension for the five pathways in this bi-dispersed sample with an effective porosity of 0.52 is $D_T = 1.10$. Wheatcraft and Tyler [11]

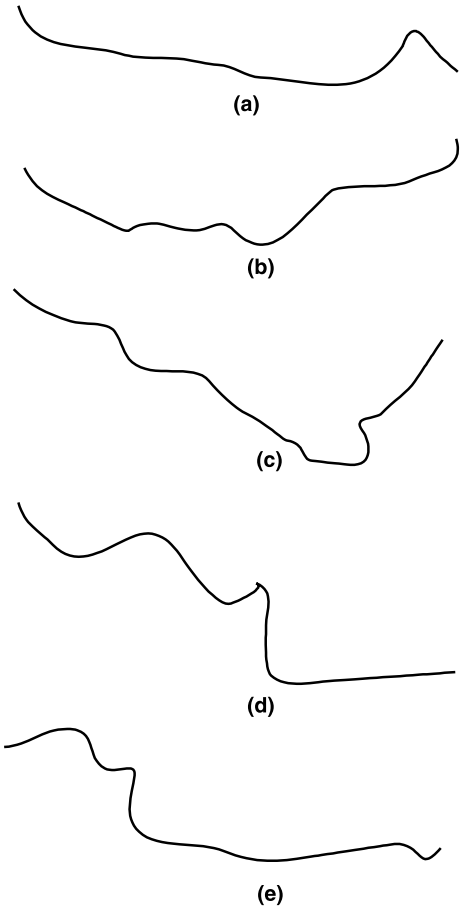

Fig. 8. Possible tortuous pathways and their tortuosity fractal dimensions for flow through a porous sample: (a) $D_T = 1.07$; (b) $D_T = 1.08$; (c) $D_T = 1.09$; (d) $D_T = 1.13$; (e) $D_T = 1.12$.

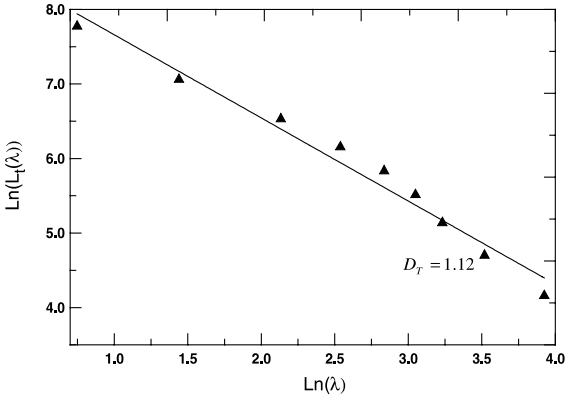

Fig. 9. Determination of tortuosity fractal dimension of a bi-dispersed porous sample with porosity of 0.52.

performed the Monte Carlo simulations on an ensemble average fractal travel distance $L_t(\lambda)$ versus scale of λ for the fractal random walk model simulating the dispersivity in heterogeneous media, and obtained the tortuosity fractal dimension of $D_T = 1.081$, which is very close to our result of $D_T = 1.10$.

7. Comparison of model predictions and permeability data

We now compare the permeability values based on the present fractal models with experimental data of Chen et al. [1] for a mono-dispersed porous sample (with $\phi = 0.49$) and three bi-dispersed porous samples (with $\phi_{eff} = 0.52,\ 0.54,\ 0.56$), respectively. Computations of Eq. (27) were carried out for $R = 0.30$ mm, $D_T = 1.1$, $d^+ = 24$ with D_f determined from Eqs. (35a) and (35b). The results are presented in Figs. 10(a) and (b) for the mono-dispersed medium and the bi-dispersed media, respectively. The dotted line in Fig. 10(a) shows that the fractal permeability model for mono-dispersed porous medium is slightly lower than experimental data [1]. In the same figure, we also plot the well known Kozeny–Carman equation [24] for the permeability of a porous bed packed with uniform spherical solid particles (a mono-dispersed porous medium):

$$K = \frac{\phi^3 d_p^2}{a(1-\phi)^2}, \tag{36}$$

where ϕ is the porosity, d_p is the particle's diameter, and $a = 180$ is an empirical constant. It is shown that the present fractal permeability model for mono-dispersed porous media (shown as a dashed line) is in better agreement with the experimental datum than the Kozeny–Carman model given by Eq. (36). Fig. 10(b) is a comparison of the present fractal permeability model for bi-dispersed media with experimental data [1]. Again, it is shown that the fractal permeability model is in good agreement with measurements. A comparison of Figs. 10(a) and (b) shows that the permeability of the mono-dispersed porous medium is much higher than that of the bi-dispersed porous medium at the same effective porosity. This is because the permeability is very sensitive to the macro-(maximum) pore size (λ_{max}), and the mono-dispersed porous medium has larger macro-pores than that of the bi-dispersed porous medium at the same effective porosity as shown in Eq. (24).

Fig. 11 shows the effects of D_f and D_T on permeabilities at various porosities. Fig. 11(a) shows that at a fixed value of D_T ($D_T = 1.2$) the permeability increases with the pore area fractal dimension D_f. The reason is that as D_f is increased, the porosity or the total pore area increases (see Fig. 7), and the permeability will reach the maximum value of $D_f = 2$ as stated in Section 4. Fig. 11(b) shows that at a fixed D_f ($D_f = 1.8$) the permeability decreases with the increase of the tortuosity fractal dimension D_T. This is because when the tortousity

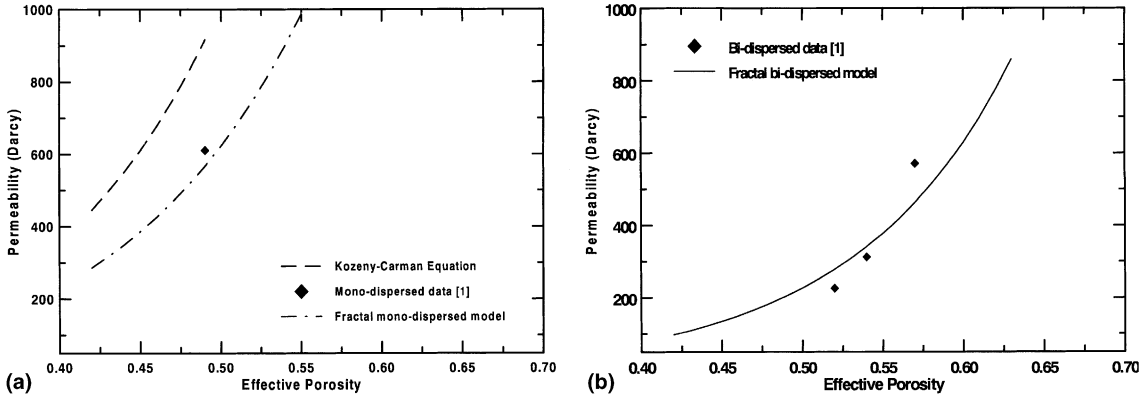

Fig. 10. A comparison of permeabilities from the present fractal model and experimental data: (a) mono-dispersed media; (b) bi-dispersed media.

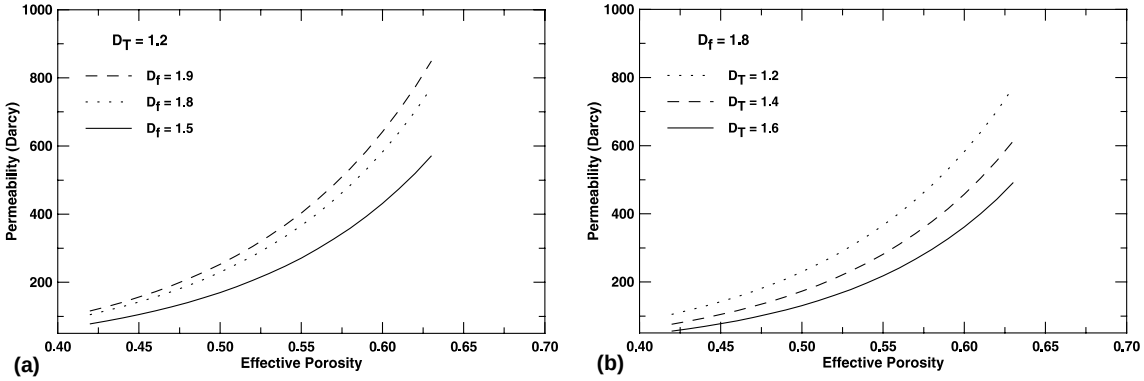

Fig. 11. Effects of D_f and D_T on permeability: (a) permeability versus D_f; (b) permeability versus D_T.

fractal dimension D_T increases, the flow pathways are more tortuous, causing more resistance for flow and lower the permeability value.

8. Concluding remarks

A fractal permeability model for bi-dispersed porous media, taking into consideration of the non-uniform pore sizes, is derived in this paper. The fractal permeability model, given by Eq. (27), is in terms of the tortuosity fractal dimension D_T, pore area fractal dimension D_f, and the structural parameters A, $\bar{\lambda}_{max}$, L_0. The last three structure parameters, given by Eqs. (21), (24)–(26) and (28), respectively, depend on the porosities of the bi-dispersed porous medium (i.e., ϕ_i and ϕ_{eff}) as well as the average size of the clusters R and the minimum particle diameter d_0. Thus, the permeability of a bi-dispersed porous medium can be written implicitly as

$$K = K(D_T, D_f, \phi_{eff}, \phi_i, R, d_0), \tag{37}$$

where the parameters ϕ_{eff}, ϕ_i, R, d_0 are determined from measurements, the fractal dimension D_T can be determined by the box-counting method, and the value of D_f can be determined based on the box-counting method and or from Eqs. (35a) and (35b). The permeability of a mono-dispersed porous medium can be considered as a special case of the bi-dispersed porous medium by setting $\phi_i = 0$. The predictions of permeabilities of mono-dispersed and bi-dispersed porous media based on the fractal model are found to be in good agreement with experimental data. This verifies the validity of the present fractal permeability model for porous media.

Acknowledgements

This work was supported by the Research Grant Council of Hong Kong Special Administrative Region through Grant Number HKUST6044/97E.

References

[1] Z.Q. Chen, P. Cheng, T.S. Zhao, An experimental study of two phase flow and boiling heat transfer in bi-dispersed porous channels, Int. Commun. Heat Mass Transfer 27 (2000) 293–302.

[2] A.J. Katz, A.H. Thompson, Fractal sandstone pores: implications for conductivity and pore formation, Phys. Rev. Lett. 54 (1985) 1325–1328.

[3] B.B. Mandelbrot, in: The Fractal Geometry of Nature, W.H. Freeman, New York, 1982, pp. 23–57 (see also pp. 117–119).

[4] T.L. Warren, D. Krajcinovic, Random Cantor set models for the elastic-perfectly plastic contact of roughness surfaces, Wear 196 (1996) 1–15.

[5] F.M. Borodich, A.B. Mosolov, Fractal roughness in contact problems, J. Appl. Math. 56 (1992) 681–690.

[6] A. Majumdar, B. Bhushan, Role of fractal geometry in roughness characterization and contact mechanics of surfaces, J. Tribol. 112 (1990) 205–216.

[7] R. Pitchumani, B. Ramakrishnan, A fractal geometry model for evaluating permeabilities of porous preforms used in liquid composite molding, Int. J. Heat Mass Transfer 42 (1999) 2219–2232.

[8] B. Ramakrishnan, R. Pitchumani, Fractal permeation characteristics of preforms used in liquid composite molding, Polym. Compos. 21 (2000) 281–296.

[9] B.M. Yu, Letters to Editors, Comments on A fractal geometry model for evaluating permeabilities of porous preforms used in liquid composite molding, Int. J. Heat Mass Transfer 44 (2001) 2787–2789.

[10] B.M. Yu, K.L. Yao, Numerical evidence of the critical percolation probability $P_c = 1$ for site problems on Sierpinski gaskets, J. Phys. A 21 (1988) 3275–3284.

[11] S.W. Wheatcraft, S.W. Tyler, An explanation of scale-dependent dispersivity in heterogeneous aquifers using concepts of fractal geometry, Water Resour. Res. 24 (1988) 566–578.

[12] M. Sahimi, in: Flow and Transport in Porous Media and Fractured Rocks, VCH Verlagsgesellshaft mbH, Weinheim (Germany), 1995, p. 13.

[13] T. Vicsek, in: Fractal Growth Phenomena, World Scientific Publishing Co. Pte. Ltd, Singapore, 1989, p. 15.

[14] A. Majumdar, Role of fractal geometry in the study of thermal phenomena, in: C.L. Tien (Ed.), Annual Review of Heat Transfer, vol. 4, Hemisphere Publishing Co., Paris, 1992, pp. 56–57.

[15] B.M. Yu, J.H. Li, Some fractal characters of porous media, Fractals 9 (3) (2001) 365–372.

[16] M.M. Denn, in: Process Fluid Mechanics, Prentice-Hall, Englewood Cliff, NJ, 1980, p. 35.

[17] A.T. Skjeltorp, in: J. Feder, A. Aharony (Eds.), Fractals in Physics, North-Holland, Amsterdam, 1990, pp. 315–321; See also, Geometrical scaling of microsphere-deposited monolayers with holes, Phys. D 38 (1989) 315–321.

[18] B.M. Yu, K.L. Yao, Properties for two-dimensional fractal aggregation in external fields, Phys. Rev. A 41 (1990) 5564–5567.

[19] A. Majumdar, Role of fractal geometry in the study of thermal phenomena, in: C.L. Tien (Ed.), Annual Review of Heat Transfer, vol. 4, Hemisphere Publishing Co., Paris, 1992, p. 87.

[20] T. Vicsek, in: Fractal Growth Phenomena, World Scientific Publishing Co. Pte. Ltd., Singapore, 1989, p. 14.

[21] E. Scheidegger, in: The Physics of Flow through Porous Media, University of Toronto, Ontario, 1963, p. 10.

[22] J. Feder, A. Aharony, Fractals in Physics, North-Holland, Amsterdam, 1989.

[23] Z.Q. Chen, P. Cheng, C.H. Hus, A theoretical and experimental study on stagnant thermal conductivity of bi-dispersed porous media, Int. Commun. Heat Mass Transfer 27 (2000) 601–610.

[24] P.C. Carman, Flow of Gases through Porous Media, ButterWorths Scientific Publications, London, 1956.